11–12 (2021) 100062

Contents lists available at ScienceDirect

Journal of Non-Crystalline Solids: X

journal homepage: www.sciencedirect.com/journal/journal-of-non-crystalline-solids-x

Thermal rejuvenation of an aged Au-based metallic glass by fast scanning calorimetry

C.M. Meylan [a], K. Georgarakis [b], A.L. Greer [a,*]

[a] Department of Materials Science & Metallurgy, University of Cambridge, 27 Charles Babbage Road, Cambridge CB3 0FS, UK
[b] School of Aerospace, Transport and Manufacturing, Cranfield University, Cranfield MK43 0AL, UK

ARTICLE INFO

Keywords:
Fictive temperature
Metallic glass
Rejuvenation
Relaxation
Ultra-fast scanning calorimetry
Mechanical properties

ABSTRACT

A metallic glass (MG) annealed above its glass-transition temperature T_g, and cooled, may show an enthalpy increase ΔH, and other property changes. The extent of this thermal rejuvenation depends on the state of the MG (represented by effective cooling rate Φ_i) and the post-anneal cooling rate Φ_c. Previous studies examined effects of (Φ_c/Φ_i) up to 10^2. With a Au-based MG aged for up to 10 years at room temperature, and using fast calorimetry to anneal and then cool at up to 5000 K s^{-1}, we extend (Φ_c/Φ_i) to 10^7. The rejuvenation is limited by anneal temperature or by Φ_c, when, for all MGs, $\Delta H/T_g$ shows a universal approximate scaling with $\log(\Phi_c/\Phi_i)$. We detect decoupling of vitrification from α relaxation, and highlight limitations in the use of fictive temperature to characterize glassy states. Rejuvenation of the Au-based MG decreases its elastic modulus and hardness, extending trends reported for other MGs.

1. Introduction

On annealing, as-cast metallic glasses (MGs) undergo structural relaxation, reaching states of lower volume and lower enthalpy. It has long been known that the relaxation-induced property changes, notably embrittlement, can be partially reversed by a second anneal at higher temperature [1–3]. In these early studies, this partial reversal was achieved with the second anneal well below the glass-transition temperature, T_g. In these cases, the glassy states show some degree of reversible ordering, but are far from the metastable (or internal) equilibrium of the supercooled liquid. Indeed, when the second anneal is continued to longer times, the initial reversal of relaxation is followed by further relaxation [1–3].

In contrast, bulk metallic glass (BMG) systems have sufficient resistance to crystallization that it is possible to explore the effects of a second anneal above T_g, i.e. in the supercooled liquid region [4]. The partial reversal of initial annealing-induced changes has now been observed for many properties: not only reduced embrittlement, but decreases in hardness, Young's modulus and density, and an increase in the heat of relaxation on temperature scanning [5–13]. A variant technique involves not an anneal above T_g, but a brief excursion enabled by ultra-fast Joule heating [14]. We consider all these effects as examples of *thermal rejuvenation* [7], taking the BMG to a higher-energy state (we do not favour the term *recovery annealing* [4], as that is more widely used for treatments that take polycrystalline metals and ceramics to lower-energy less-defective states). Recently, thermal rejuvenation (TR) was applied to introduce a gradient in hardness and stored energy across the diameter of a BMG rod [15]. When loading the rod under compression, this 'tailored hardening' blocked shear bands from traversing the whole rod, and led to apparent work-hardening throughout the entire plastic deformation. The atomistic aspects of thermal rejuvenation have been examined in molecular-dynamics simulations [14,16].

Saida et al. [7] have quantitatively analysed the conditions for TR. MG samples were relaxed by annealing at T_g and then cooled at a controlled rate Φ_i which was used to characterize the relaxed state. The second anneal was at temperature T_a and was followed by cooling at Φ_c. For the MG systems studied, a *rejuvenation map* was constructed, showing the boundary between rejuvenation and relaxation as a result of the second anneal [7]. The axes on the map are Φ_c/Φ_i and T_a/T_g. The map shows that, roughly, rejuvenation is achieved if $\Phi_c/\Phi_i > 1$ and $T_a/T_g \geq 1.2$. In the present work, we examine these conditions further. We use T_a/T_g in the range 0.9 to 1.2. We also extend the effective range of Φ_c/Φ_i to much higher values. Rather than focusing on the changes from the relaxed state, we quantify the absolute limits of the rejuvenated state achievable in two distinct regimes: limited by T_a, or limited by Φ_c.

In the present work, TR is carried out by fast-scanning calorimetry

* Corresponding author at: University of Cambridge, Department of Materials Science & Metallurgy, 27 Charles Babbage Road, Cambridge CB3 0FS, UK.
E-mail address: alg13@cam.ac.uk (A.L. Greer).

https://doi.org/10.1016/j.nocx.2021.100062
Received 24 March 2021; Received in revised form 30 May 2021; Accepted 31 May 2021
Available online 2 June 2021

(FDSC) that allows for high Φ_c. The MG is a Au-based melt-spun ribbon aged for 8 (and 10) years at room temperature (RT), making it very well relaxed, with a correspondingly low effective value of Φ_i. The degree of rejuvenation is determined in terms of increase in enthalpy and in fictive temperature, measured by FDSC; and by the change in mechanical properties, measured by instrumented indentation (nanoindentation). We review the literature on TR of MGs, and we show that, using FDSC, the reported effects can be far exceeded. The difficulties in defining Φ_i for the well-aged samples may relate to the recently reported decoupling of vitrification from α relaxation in the same Au-based MG [17].

2. Experimental methods

2.1. Sample preparation

An alloy of nominal composition $Au_{49}Cu_{26.9}Si_{16.3}Ag_{5.5}Pd_{2.3}$ (at.%) was prepared from high-purity elements (≥99.9%) in an arc-melter under argon atmosphere; titanium was used as an oxygen getter. The ingot was inverted and re-melted five times to achieve chemical homogeneity. Melt-spinning (on to a copper wheel rotating with peripheral speed 33 m s^{-1} under helium atmosphere) was used to prepare a 40-μm-thick fully glassy ribbon. Samples from this ribbon were studied after eight and ten years of storage at RT, which is ~0.75 of T_g (=391 K, measured on heating at 0.33 K s^{-1}). Samples from the same ribbon have been characterized in earlier work ([18]; Supplementary Materials of Ref. [19]): X-ray diffraction shows that the ribbon is glassy after production, and after years of storage at RT. Polishing reveals that the ribbons contain some internal pores, 100–200 μm long, 50 μm wide, and estimated to be ≤10 μm deep.

2.2. Fast differential scanning calorimetry

Ribbon for FDSC measurements was polished down from both sides to a thickness < 20 μm, then cut by a scalpel into pieces of a maximum size of 150 × 150 μm^2 (estimated mass 1–2 μg). A Flash DSC 1 (Mettler Toledo) was operated with a UFS 1 sensor. The system was purged with nitrogen at 30 ml min^{-1} and the sample-support temperature was set to 233 K. Temperature calibration of the sensor was performed by measuring the melting point of indium and the ferromagnetic Curie temperature of nickel. Heat-flow curves of the aged and thermally rejuvenated samples were measured by heating from 233 K to 773 K at 100 K s^{-1}, then cooling back to 233 K at the same rate, followed by a second heating run to obtain the baseline. The effect of thermal lag was found here to be negligible for heating at 100 K s^{-1} and therefore not considered.

2.3. Thermal rejuvenation

Rejuvenation was mainly performed by FDSC using the following heating protocol: heating from 233 K to a temperature T_a (ranging from 343 K to 468 K) at 100 K s^{-1}, isothermal holding at T_a for a time t_a (ranging between 0.1 s and 3 h), then cooling at 100 K s^{-1} back to 233 K. Other cooling rates, 2 K s^{-1}, 1000 K $s^{-1}$and 5000 K s^{-1}, were also tested for certain T_a. Thermal rejuvenation was also performed on a macroscopic sample (~2 cm-long piece of ribbon) to permit mechanical-property measurements. The ribbon was dipped for 10 s into sunflower oil at 423 K (heated on a hot plate), then quenched in water at around room temperature, followed by cleaning in an ultrasonic bath. One end of the sample was cut off for FDSC measurement, the rest was characterized by instrumented indentation.

2.4. Instrumented indentation

Instrumented indentation was performed at RT on a XP Nanoindenter (MTS Systems Corp.) with a diamond spherical indenter of tip radius R = 8 μm under a controlled loading and unloading rate of 0.5 mN s^{-1}. The maximum thermal drift rate was set to 0.07 nm s^{-1}. Indentation was performed on the 2 cm-long ribbon piece in its aged state and after TR (8–28 h afterwards). Before indentation, the ribbon was ground, then polished with 1 μm diamond paste and finally with a 0.06 μm colloidal silica suspension. The numbers of indents were 89 on the sample in its aged state, and 38 after TR. A spacing of at least 20 μm was kept between indents.

The initial yield load F_y is defined as the load at the first pop-in (displacement burst), which was identified from the first peak in indenter tip velocity correlating with a deviation of the load-displacement curve from the Hertzian equation for elastic displacement of $F = (4/3)E_r R^{1/2} h^{3/2}$ [20], where F is the force, h the tip displacement and E_r the indentation (reduced) modulus. The initial yield pressure is calculated from $P_y = F_y/(\pi R h_y)$, where h_y is the displacement at the first pop-in. By inserting F_y and h_y into the Hertzian equation, E_r is determined. The Young modulus E is calculated using the relation $1/E_r = (1-\nu_i^2)/E_i + (1-\nu^2)/E$, where E_i = 1141 GPa and ν_i = 0.07 are the Young modulus and Poisson ratio of the indenter tip, respectively, and ν = 0.406 [21] is the Poisson ratio of the sample. The hardness is calculated using $H = F_{max}/(\pi a^2)$, with the maximum indentation load F_{max} = 50 mN, the contact radius $a = \sqrt{2Rh_c - h_c^2}$ and $h_c = (h_{max} + h_f)/2$ [22]; h_{max} is the maximum displacement and h_f the depth of residual impression. The initial pop-in size Δh is defined as the increase in displacement at constant load during the first pop-in.

3. Results

3.1. Fictive temperature and enthalpy

The heat-flow trace of the Au-based ribbon aged for eight years at RT, measured at 100 K s^{-1} by FDSC, shows a large overshoot overlapping with the glass transition (Fig. 1a). With the construction shown, T_g is estimated to be ~418 K, significantly higher than the 391 K measured in conventional DSC at 0.33 K s^{-1}. The onset of crystallization is at ~480 K. Endothermic overshoot peaks are characteristic for an annealed glass, and occur when the glass is heated at a higher rate than its *effective cooling rate* (Φ_{eff}), which is the rate at which the melt would need to be quenched in order to form a glass of an equivalent energetic state. A well relaxed glass, such as the present RT-aged ribbon, has a lower Φ_{eff} than a freshly melt-spun, highly unrelaxed glass. The overshoot in Fig. 1a is remarkably large because the MG is not only well aged, but also heated at a high rate. Upon heating this MG at lower rates, e.g. 0.33 K s^{-1}, a sub-T_g endotherm (also known as a *shadow glass transition*, and corresponding to disordering of relaxed zones [23,24]) occurs instead of an overshoot (inset of Fig. 1a).

The fictive temperature (T_f) can be used to characterize glassy states, and corresponds to the temperature at which the extrapolations of the glass and supercooled-liquid enthalpy lines intersect (Fig. 1b). Using the equal-area construction [24,25], T_f can be determined from the FDSC heat-flow trace (see hatched areas in Fig. 1a), and is 363 ± 3 K for the MG ribbon aged for 8 years at RT. This value is well below the onset $T_g \approx$ 418 K upon heating at 100 K s^{-1} (and even below $T_g \approx$ 391 K).

Upon annealing at a temperature T_a, the glass is expected to relax towards the equilibrium state of the supercooled liquid at that temperature, and T_f of the MG should evolve towards T_a. If T_a is lower (higher) than T_f of the initial glassy state, the enthalpy of the MG decreases (increases). Therefore, in order to achieve rejuvenation, T_a was chosen to be above T_f of the aged ribbon (but not necessarily above its T_g), and the isothermal hold for a time t_a was followed by quenching. After such a thermal treatment, the overshoot peak has a reduced height (Fig. 1a), confirming rejuvenation of the sample. The degree of rejuvenation is quantified in terms of the increase in T_f.

The degree of rejuvenation can also be quantified using the overall increase in enthalpy (ΔH). As the mass of the samples studied in FDSC is not known accurately, absolute values for ΔH could not be measured

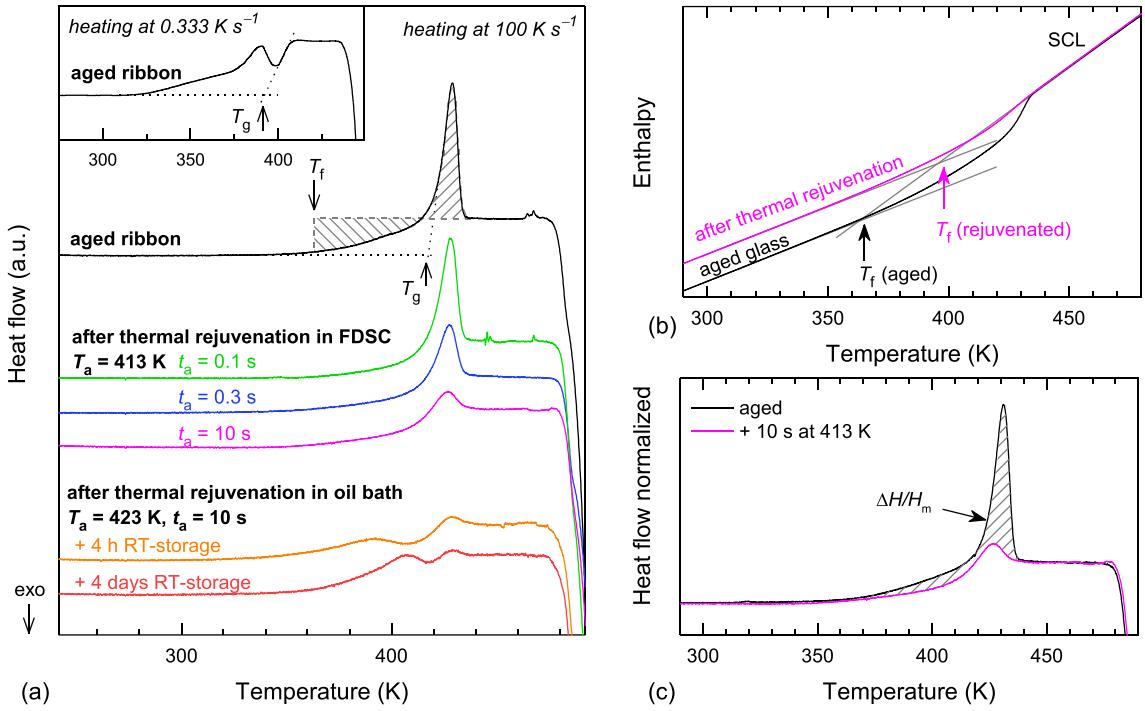

Fig. 1. (a) Example heat-flow trace measured at 100 K s^{-1} of the aged Au-based MG ribbon in its initial state, after thermal rejuvenation in FDSC (at 413 K for various times t_a, followed by quenching at 100 K s^{-1}) and after thermal rejuvenation in oil and water quenching, followed by RT-storage for approximately 4 h and 4 days. The inset shows the heat-flow trace of the aged ribbon on heating at 0.33 K min^{-1} by conventional DSC. An example of the determination of the fictive temperature T_f via the equal-area construction is shown in the case of the aged sample by the hatched areas. (b) Enthalpy-temperature plot of the aged ribbon and after thermal rejuvenation (based on measured data [18]). The intersection of the supercooled liquid (SCL) enthalpy line with that of the glass corresponds to T_f. (c) The normalized increase in enthalpy $\Delta H/H_m$ determined as the area (hatched) between the curves of the aged ribbon in its initial state and after thermal rejuvenation (10 s at 413 K, cooled at 100 K s^{-1}), after normalization of the curves to their heat of melting H_m.

directly. Instead, the change in enthalpy is normalized to the heat of melting (H_m). Values of $\Delta H/H_m$ were determined as the area between the curves of the aged and rejuvenated samples (see Fig. 1c), after the curves had been normalized to the areas of their melting peaks. The increases in T_f and in enthalpy are of course linked (Fig. 1b), but they show distinct measurement uncertainties. Values of T_f can be determined more precisely; values of $\Delta H/H_m$ show more scatter (Fig. 2), but more accurately reflect the degree of rejuvenation.

For the ribbon aged for 8 years at RT, Fig. 2 shows the increases in T_f and $\Delta H/H_m$ after TR at various T_a and t_a, followed by quenching at 100 K s^{-1}. The maximum increases are ~30 K for T_f, and 0.13–0.15 for $\Delta H/H_m$. Absolute values for the increase in enthalpy can be estimated, given a value for H_m; taking $H_m = 5.39$ kJ mol^{-1} [19] for this MG composition, the maximum increase in ΔH is 0.7–0.8 kJ mol^{-1} (right-hand scale in Fig. 2b). On annealing at ≥433 K for more than 10 s, the onset temperature and heat of crystallization both decrease, suggesting partial crystallization; therefore annealing was kept to below this temperature. Contrary to expectation, some rejuvenation is observed even for $T_a \leq$ 363 K, which is at or below the T_f of the aged ribbon; this is discussed in §4.1. The progress in rejuvenation during an anneal at a given temperature is most clearly seen in the T_f data (Fig. 2a). For all except the lowest values of T_a, the observed increases saturate within the measured range of t_a, as indicated by the sketched curves. At higher T_a, the increase in T_f is faster and reaches saturation sooner. The saturation value of T_f also increases with T_a, but this effect appears to saturate for T_a between 403 K and 413 K.

These trends were examined further for the Au-based MG ribbon aged for a further two years at RT, which caused its T_f to decrease to 347

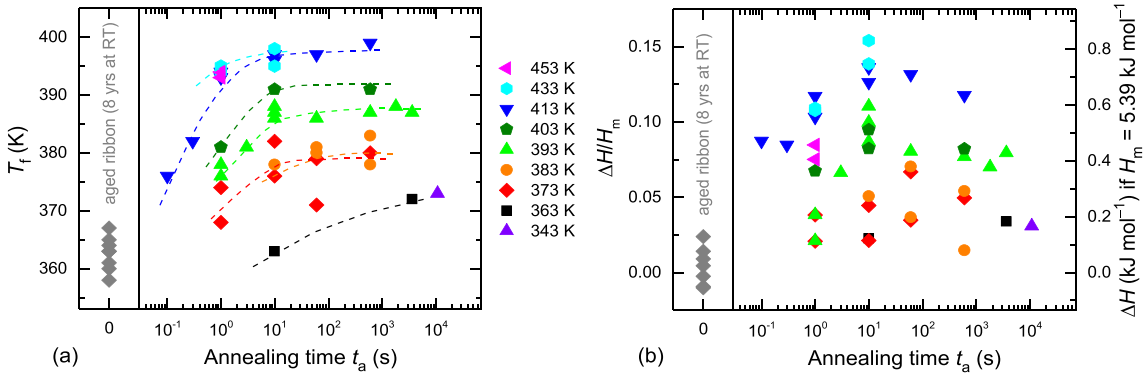

Fig. 2. The increase (a) in fictive temperature T_f and (b) in enthalpy $\Delta H/H_m$ of the 8-yr-aged ribbon after thermal rejuvenation at different temperatures and times, followed by cooling at 100 K s^{-1} by FDSC. The dashed lines in (a) are a guide for the eyes.

± 2 K. To increase the achievable degree of rejuvenation, a higher T_a (up to 468 K) and higher cooling rates Φ_c (1000 K s^{-1} and 5000 K s^{-1}) were applied to this ribbon (the effect of a lower Φ_c of 2 K s^{-1} was also tested). The measured increases in T_f and in $\Delta H/H_m$ are shown in Supplementary Material Fig. S1. There is again evidence for the saturation of rejuvenation at long enough t_a. The key new result is that the saturation extent of rejuvenation is greater for higher Φ_c. With Φ_c = 5000 K s^{-1}, T_f increased by up to ~85 K and $\Delta H/H_m$ increased by 0.22, which corresponds to an estimated enthalpy increase of ~1.2 kJ mol^{-1}. With Φ_c = 100 K s^{-1} (Fig. S1e), again, even annealing at a T_a slightly above (353 K) or well below (333*K*) the T_f of the 10-yr-aged ribbon led to some rejuvenation (§4.1).

The data on TR of the ribbon after 8 years and after 10 years at RT are combined in Fig. 3, which shows the saturation values of T_f as a function of T_a for four values of Φ_c. At a given Φ_c, the saturation value of T_f as a function of T_a shows two regimes, as seen for example in the data for Φ_c = 5000 K s^{-1} (green triangles). During the rejuvenation anneal itself, T_f is expected to become equal to T_a, and that is seen for the lower T_a values in this dataset. A second regime is entered at the highest T_a values, when the attained T_f appears to saturate. Comparing the different datasets, the saturation value of T_f is higher for higher Φ_c. For a melt of a given composition, the rate Φ_c at which it is cooled determines the temperature at which it freezes into a glass. Monnier et al. [17] measured T_f of the MG (of the same composition as studied here) quenched at various rates from the melt: the T_f values of the MG formed at cooling rates of 2, 100, 1000 and 5000 K s^{-1} are shown by solid horizontal lines in Fig. 3. Without any adjustable parameters, the line for Φ_c = 5000 K s^{-1} is in reasonable agreement with the present T_f values measured after cooling at the same rate after the rejuvenation anneal. Thus, it is possible to achieve glassy states of the same T_f upon TR as upon quenching from the equilibrium melt.

For lower values of Φ_c, however, there is a progressive discrepancy in the limiting values of T_f: at Φ_c = 2 K s^{-1}, the expected T_f ≈ 407 K [17], whereas the limiting value in the present work is 382 K. The origin of the discrepancy is explored in §4.2.

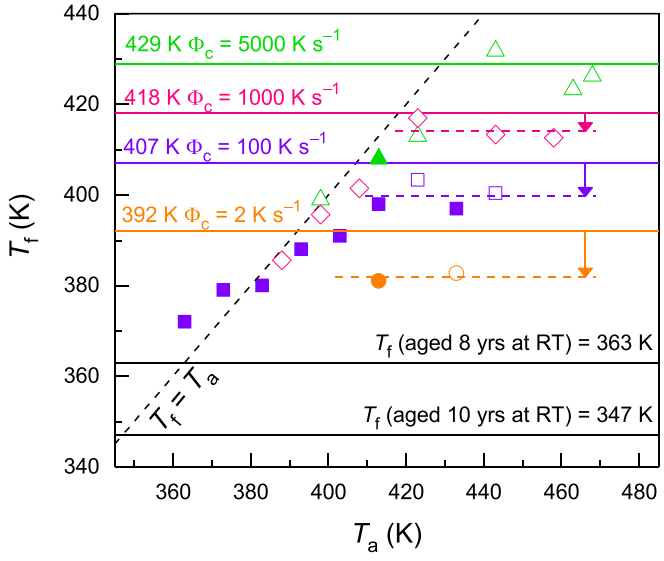

Fig. 3. Estimation of saturation values of T_f as a function of the rejuvenation temperature T_a. The cooling rate Φ_c after annealing is 2 K s^{-1} (orange circles), 100 K s^{-1} (violet squares), 1000 K s^{-1} (pink diamonds) and 5000 K s^{-1} (green triangles). The full data points were measured on the 8-yr-aged ribbon and the open points on the 10-yr-aged ribbon. The solid lines at 392 K, 407 K, 418 K and 429 K correspond to the expected T_f for a glass formed upon quenching the melt at 2 K s^{-1}, 100 K s^{-1}, 1000 K s^{-1}, and 5000 K s^{-1}, respectively, according to Monnier et al. [17]. (For interpretation of the references to colour in this figure legend, the reader is referred to the web version of this article.)

3.2. Indentation modulus and hardness

The effect of TR on the mechanical properties of the aged ribbon was determined by instrumented indentation (§2.4). A 2 cm-long piece of the 8-yr-aged ribbon, was annealed in oil at 423 K for 10 s, then quenched in water (at an estimated Φ_c of 30–200 K s^{-1}). The set-up and indentation measurements took place over several hours; the indents were performed 8–28 h after annealing. During this time, the annealing-induced rejuvenation was partially reversed by relaxation, as RT is quite high relative to T_g of this MG composition (~0.75 T_g). Heat-flow traces from this ribbon were measured 4 h and 4 days after the oil-annealing, i.e. before and sometime after the indentation (Fig. 1a). The overshoot peak decreased in height, which confirms that the ribbon was rejuvenated by the oil-annealing, but a sub-T_g endotherm appeared at ~400 K after 4 h at RT, and became larger after 4 days, a sign of subsequent relaxation. After 4 h at RT, T_f ≈ 386 K and $\Delta H/H_m$ ≈ 0.066, and after 4 days, T_f ≈ 385 K and $\Delta H/H_m$ ≈ 0.036.

Examples of instrumented-indentation load-displacement curves are

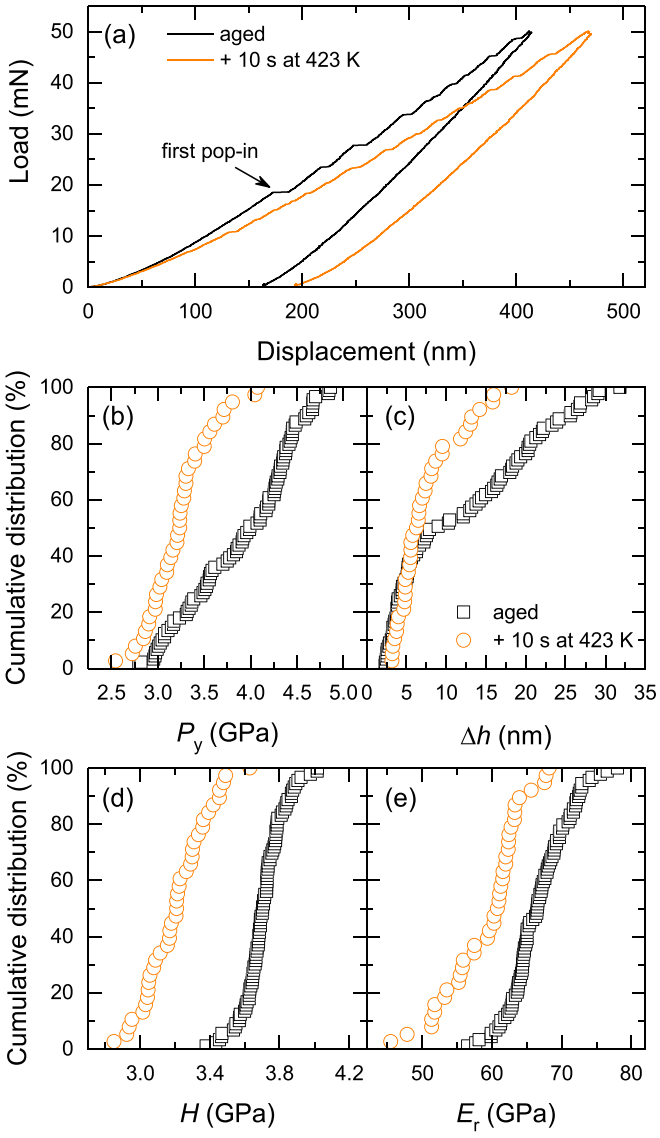

Fig. 4. Instrumented indentation of the 8-yr-aged ribbon before and after rejuvenation in oil at 423 K followed by quenching in water. (a) Example instrumented-indentation load–displacement curves. Cumulative distribution curves of: (b) initial yield pressure P_y; (c) initial pop-in size Δh; (d) hardness H; and (e) indentation modulus E_r.

given in Fig. 4a for the 8-yr-aged ribbon before and after TR. Discrete pop-ins occur during loading, which represent the initiation and propagation of shear events [26]. The first pop-in marks the onset of yield, and occurs at the initial yield pressure P_y. Further properties measured from indentation are the initial pop-in size Δh, which is correlated to the speed of the indenter tip during the first pop-in [27], the hardness H, and indentation modulus E_r. The results for all the indents are summarized in the form of cumulative distribution curves (Fig. 4b–e). The spread in values is considered to represent a true variation in local properties of the MG [28]. The properties can be described in terms of their median values. The values for H measured here by instrumented indentation are similar to the reported Vickers hardness of 360 Hv (≈3.5 GPa) [21]. The median $E_r \approx 67$ GPa of the aged ribbon corresponds to a Young modulus of $E \approx 59$ GPa, which is considerably lower than the expected $E = 74.4$ GPa from ultrasonic measurements [21]. The reason for this difference is not known, though it is likely to be internal pores in the present ribbon sample (§2.1).

After TR, a general softening of the aged ribbon was observed: the median values of P_y, H and E_r decreased by 19%, 13% and 8%, respectively. In the case of H and E_r, the entire distribution curves are shifted to lower values. In the case of P_y and Δh, in contrast, the upper parts of the distributions are affected most, whereas the lower values decreased less (for P_y), or not at all (for Δh).

4. Discussion

4.1. Spectrum of relaxation times

As already noted for the ribbon aged for 8 years (Fig. 2a) and 10 years (Fig. S1e) at RT, annealing can induce an increase in T_f, even when T_a is close to or below the T_f of the aged ribbon. This unexpected increase in T_f is likely to be related to the *memory effect* that is seen when the structural changes in a MG show a spectrum of relaxation times [29]. We consider a MG property (measured at RT) that increases because of structural relaxation during an isothermal anneal. As shown schematically in Fig. 5a, annealing at a lower temperature T_1 gives an increase that is slower, but ultimately greater in extent, as the sample tends towards internal equilibrium at T_1. The behaviour of interest is when, as shown, the anneal at T_1 is stopped at time t_1 when the property reaches its internal equilibrium value for the higher temperature T_2 and then the anneal is continued at T_2. In a simple model, the property value should simply remain stable at the equilibrium value for T_2, but it shows the more complex behaviour of first decreasing and then reverting to the equilibrium value.

The actual continuous spectrum of relaxation times can be represented most simply by considering the behaviour of the MG to be governed by just two relaxation processes: fast and slow [29]. As shown in the left-hand inset in Fig. 5a, the measured property increase is an average of values given by the fast and slow processes (Fig. 5a and b). When the annealing temperature is changed from T_1 to T_2 at time t_1, the subsequent opposing evolution of the fast and slow processes gives the observed complex behaviour (right-hand inset in Fig. 5a).

In the present case, the T_f can be regarded as analogous to the property in Fig. 5a, but one that decreases with relaxation rather than increasing. When the Au-based MG is aged at RT, its decreasing T_f is an average of the values given by fast (minority) and slow (majority) processes (Stage 1 in Fig. 5b). On annealing at T_a, which is below T_f of the aged MG, the response of the fast and slow processes is such that the measured T_f of the MG increases (Stage 2). Ultimately, on holding for sufficient time at T_a, the T_f of the MG decreases towards T_a (Stage 3). The rapid rise and slow fall of T_f in Stages 2 and 3 is analogous to the rapid fall and slow rise of the property after time t_1 in Fig. 5a. Such effects show the limitations of T_f for characterizing the state of a glass.

The basis for memory effects has been studied for a wide range of glass categories. As reviewed by Scalliet and Berthier, such effects are generally taken to indicate a hierarchy in both the time- and length-scales associated with a complex free-energy landscape [30]. Memory effects have been thoroughly studied in the present Au-based MG [31]; the authors suggest that the 'fast' and 'slow' processes correspond, respectively, to β (secondary) and α (primary) relaxation, in each case involving distinctive collective atomic motions. The implications of a broad spectrum of relaxation times are explored further in the next section.

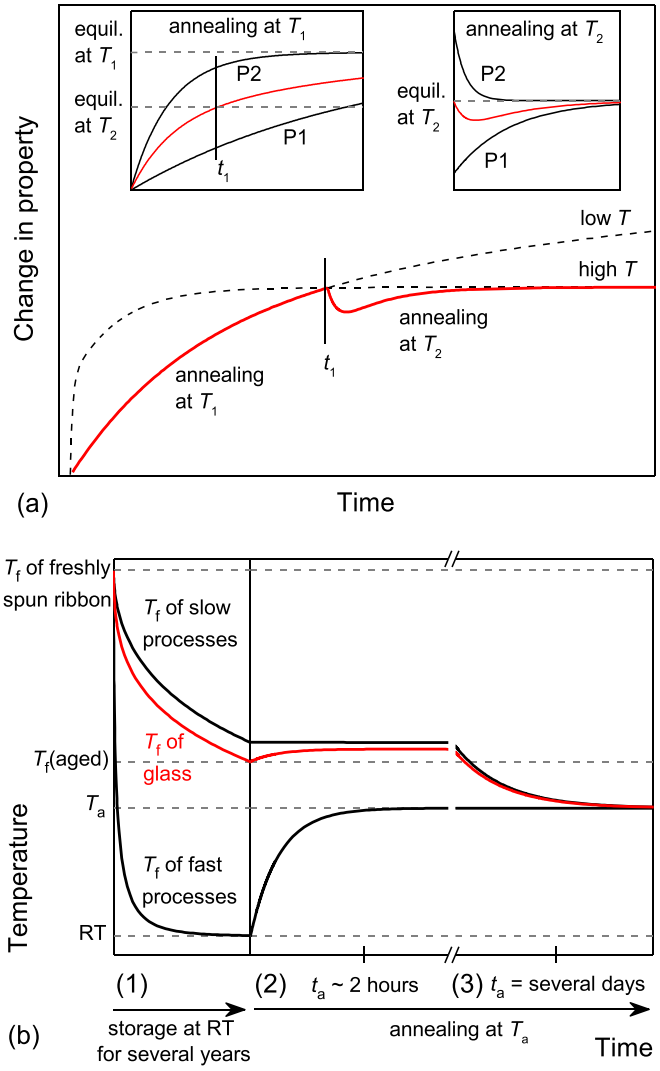

Fig. 5. (a) Schematic diagram of the memory effect in structural relaxation of a MG. The relaxation is taken to involve fast and slow processes. As explained in the main text, crossover annealing (first at T_1, then at T_2) gives complex non-monotonic property evolution (right-hand inset). (b) Schematic diagram of proposed analogous effects for the T_f of the Au-based MG in the present work. During relaxation of the MG at RT (1), the overall T_f decreases significantly, but the effective T_f of the fast processes has decreased much more. During thermal rejuvenation at temperature $T_a \leq T_f$ (aged) (2), the fast processes reverse while the slow processes barely change in the short timescale, giving a rise in overall T_f. If annealing at T_a were continued (3), the T_f of both fast and slow processes, and of the MG overall, would eventually reach T_a.

4.2. Decoupling of vitrification from α relaxation

This decoupling has been explored, for the present Au-based MG, by Monnier et al. [17]. Their data for the temperature dependence of the α-relaxation time (determined from a variety of techniques) are shown in Fig. 6. This is analogous to Fig. 3 in Ref. [17], but is in the form of an Angell plot, with the reciprocal temperature scale normalized with

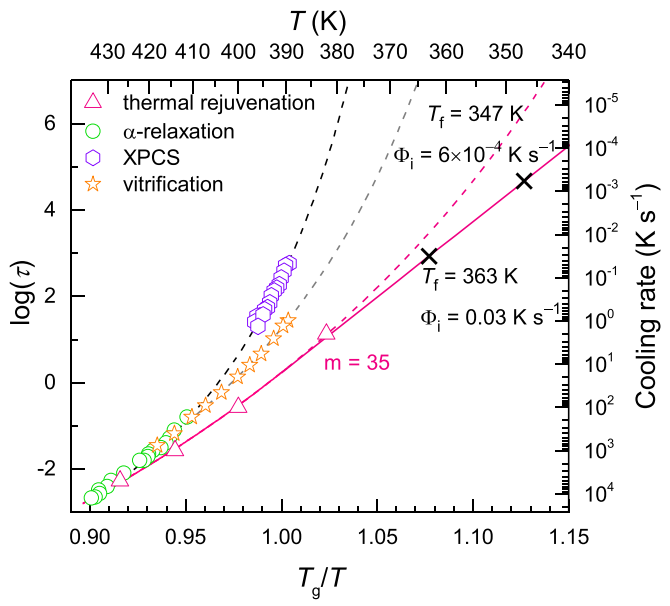

Fig. 6. Angell plot of relaxation time τ as a function of inverse temperature T, normalized to T_g = 391 K, showing data from Ref. [17]: for α-relaxation measured using FDSC (circles) and X-ray photon correlation spectroscopy (hexagons) and for vitrification upon cooling of the melt from T_f measurements by FDSC (stars). The τ for vitrification is obtained from cooling rate Φ using the relationship $\tau = \Delta T/\Phi_c$, where ΔT is the width of the glass transition [17]. The T_f values achieved in the present work by thermal rejuvenation of the aged ribbon are shown for comparison (triangles). VFT-fitting of these points (dashed red line) gives a fragility m of 35. The effective cooling rates Φ_i for the 8-yr-aged ribbon ($T_f \approx$ 363 K) and 10-yr-aged ribbon ($T_f \approx$ 347 K) are estimated using linear extrapolation (of slope m = 35) below T_g. (For interpretation of the references to colour in this figure legend, the reader is referred to the web version of this article.)

respect to T_g = 391 K (the value for the 8-yr-aged MG heated at the conventional 0.33 K s^{-1}). In vitrification, the relaxation time τ can be taken to be inversely proportional to the cooling rate of the liquid. When Monnier et al. measured the T_f of MG samples formed by cooling the liquid at different rates, they found that the characteristic values of τ matched those for α-relaxation at high temperatures ($T > 1.05\ T_g$), but progressively diverged at lower temperatures. In effect, each sample has a value of T_f that is lower than would be expected from the α-relaxation curve. The samples are more relaxed than expected, and this is related to a broad glass transition, with a spectrum of relaxation times.

Monnier et al. [17] note that decoupling is expected also in glasses 'subjected to extremely long annealing', but they cite only an example of quasistatic cooling (at 10^{-4} K s^{-1}) of a bulk polymeric system [32]. The present work allows us to explore this route to decoupling in the MG studied by Monnier et al. After TR, we find T_f values lower than those of Monnier et al. for the same cooling rate. The deviation (arrowed in Fig. 3) is plotted in Fig. 6, and shows even greater decoupling of vitrification from α relaxation. These samples have been relaxed by ageing for a long time at RT, and then thermally rejuvenated by an anneal. The implication is that, despite an apparent saturation in T_f during the anneal, the time is not sufficient to bring the MG to internal equilibrium at the anneal temperature: the MG retains some 'memory' of its more relaxed characteristics after long ageing at RT. Substantially longer anneal times t_a should reduce this memory effect, but these are limited by the need to avoid crystallization not only during annealing, but also during subsequent cooling.

The heating rate (100 K s^{-1}) used to determine T_f in the present work is different from that (1000 K s^{-1}) used by Monnier et al. The value of T_f given by the equal-area construction should be independent of heating rate, and we have verified that this is so in our own measurements up to 1000 K s^{-1}. The greater deviation (decoupling) seen in Figs. 3 and 6 is not attributable to the heating rate used to determine T_f.

The present data for the thermally rejuvenated MG samples lie on a curve in Fig. 6 that corresponds to a liquid *fragility* ($m = \mathrm{d}\log\tau/\mathrm{d}(T_g/T)_{T=Tg}$) [33] of ~35. We need to extrapolate to the lower T_f values of the RT-aged samples in order to estimate their effective cooling rates. Using a linear extrapolation as shown, $\Phi_i = 3 \times 10^{-2}$ K s^{-1} for the 8-yr-aged sample and 6×10^{-4} K s^{-1} for the 10-yr-aged sample.

4.3. Comparative extent of thermal rejuvenation

TR has been reported for several MGs and a few oxide glasses. We compare the extent of rejuvenation in these studies and in the present work. The rejuvenation is characterized by the increase in enthalpy ΔH of samples cooled at Φ_c relative to the initial state cooled at Φ_i. The tangent at T_g to the curve in an Angell plot has the gradient m, according to which the ratio T_g/T_f (and for values close to one, also T_f/T_g) is expected to vary linearly with logΦ. In these ratios, T_g is the value of T_f at the conventional cooling rate of 0.33 K s^{-1}. As can be seen in Fig. 1b, the ΔH between two glassy states is linearly proportional to the difference in their T_f values. As shown in Suppl. Mater. §S2, overall it is expected that $\Delta H \approx (T_g \Delta C_p/m)\ \log\ (\Phi_c/\Phi_i)$. For MGs, the value of m does not vary greatly, and we assume that $\Delta C_p/m$ is roughly constant. (For glasses in general, a smaller ΔC_p may be correlated with a smaller m [33].) Within the term $(T_g \Delta C_p/m)$, the greatest variability is shown by T_g, which ranges from 391 K (for the present MG) up to 825 K for the other MGs being compared.

Accordingly, we plot ΔH normalized to T_g as a function of $\log(\Phi_c/\Phi_i)$ (Fig. 7). For the wide range of compositions studied, the expected roughly linear behaviour is found. Apart from $(TeO_2)_{0.45}(V_2O_5)_{0.55}$, the oxide glasses [34] in this collection of data follow the same trend as the MGs, even though they are expected to have lower m values. The published data explore TR up to $(\Phi_c/\Phi_i) \approx 10^2$. In the present work with a combination of the higher Φ_c attainable in FDSC and the lower Φ_i attainable in well aged samples, we extend the rejuvenation up to $(\Phi_c/\Phi_i) \approx 10^7$ and achieve higher values of $\Delta H/T_g$. Our maximum increase in enthalpy is for the 10-yr-aged MG cooled at 5000 K s^{-1}: $\Delta H \approx$ 1200 J mol^{-1}. For the 8-yr-aged MG, the maximum ΔH is ~700 J mol^{-1}, not much greater than the $\Delta H \approx$ 620 J mol^{-1} reached by Saida et al. for a Zr-based MG after TR with Φ_c/Φ_i = 25.6. The logarithmic behaviour implies diminishing returns as Φ_c is increased. The dashed trend line in Fig. 7 has a gradient of 0.41 J mol^{-1} K^{-1}; this is moderately close to the value of 0.54 J mol^{-1} K^{-1}, expected for the present Au-based MG, for which T_g = 391 K, ΔC_p = 18.8 J mol^{-1} K^{-1} [35] and m = 35 (Fig. 6).

Fig. 7 shows that thermal rejuvenation can be greatly extended, but the present technique, involving μg-scale samples quenched in FDSC, is not applicable to the treatment of MG components. Thermal rejuvenation of larger samples is possible, however, and is facilitated by fast heating; this has been achieved by electrical current pulse [14] and by infra-red irradiation [13]. In these studies, the cooling-rate ratio (Φ_c/Φ_i) has not been determined, and so the results for enthalpy increase are not included in Fig. 7; the maximum values of $\Delta H/T_g$, however, are 0.29 and 0.67 J mol^{-1} K^{-1}, lying well within the range of other earlier studies. Similarly (see next section), the mechanical property changes [14] lie well within the range of other earlier studies. Nevertheless, innovative processing may allow useful thermal rejuvenation of samples much larger than in the present work.

4.4. Thermal rejuvenation of mechanical properties

As noted in §1, potential improvement in mechanical properties is a key reason for interest in TR. Using results from indentation experiments, we consider the change in elastic modulus E and hardness H induced by TR, normalized to the properties of the original relaxed state. These relative changes are compared for published data and the present work (Fig. 8). We estimate (see Suppl. Mater. §S3) that Φ_c/Φ_i for the oil-

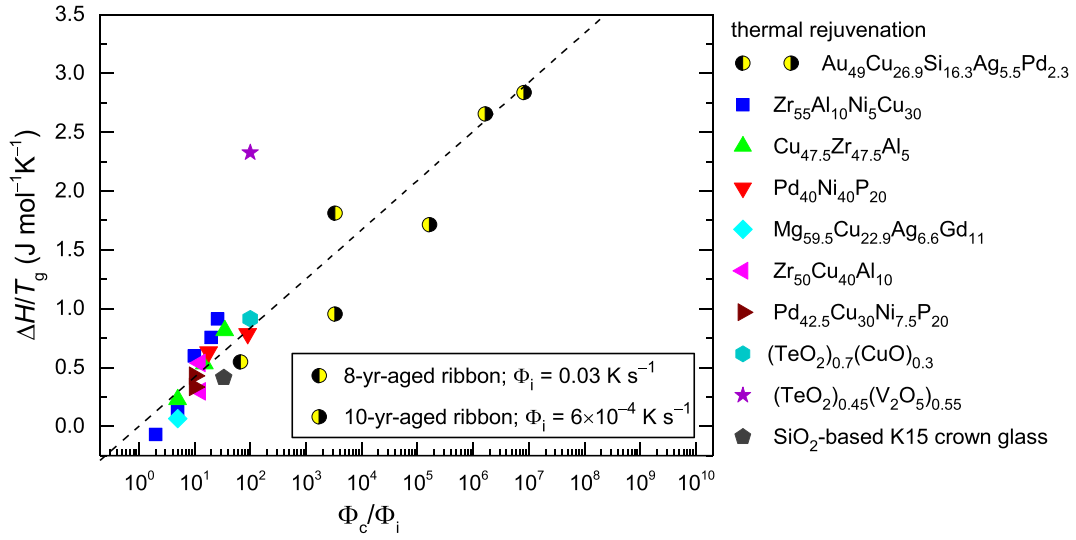

Fig. 7. Thermal rejuvenation shown as the increase in enthalpy ΔH normalized to T_g, as a function of the cooling-rate ratio Φ_c/Φ_i. Data for the aged Au-based ribbon in the present work are compared to those for other MGs $Zr_{55}Al_{10}Ni_5Cu_{30}$ [7], $Cu_{47.5}Zr_{47.5}Al_5$ [10], $Pd_{40}Ni_{40}P_{20}$ [9], $Mg_{59.5}Cu_{22.9}Ag_{6.6}Gd_{11}$ [12], $Zr_{50}Cu_{40}Al_{10}$ [8,11], $Pd_{42.5}Cu_{30}Ni_{7.5}P_{20}$ [11], and for $(TeO_2)_{0.7}(CuO)_{0.3}$ [34], $(TeO_2)_{0.45}(V_2O_5)_{0.55}$ [34] and SiO_2-based K15 crown glass [34]. The dashed line is a guide for the eye.

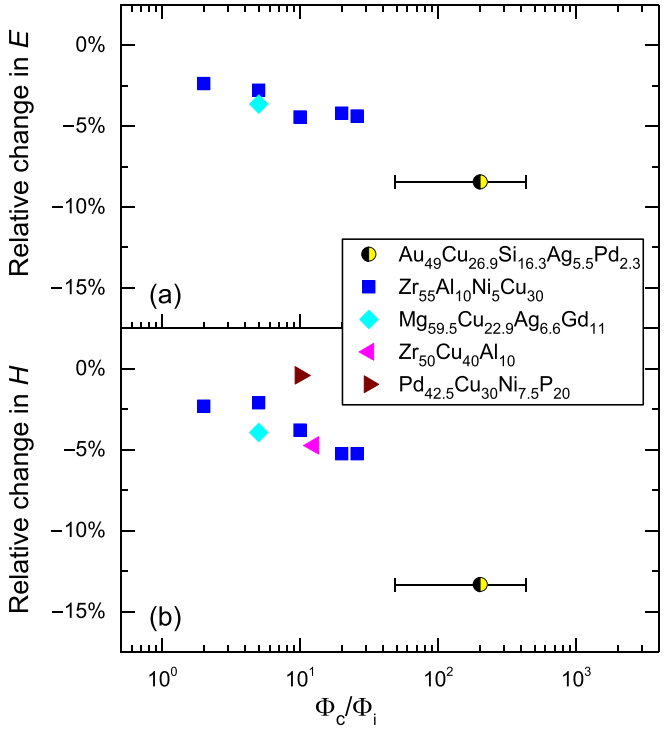

Fig. 8. Indentation measurements of the relative decrease in elastic modulus E (a) and hardness H (b) upon thermal rejuvenation, as a function of the cooling rate ratio Φ_c/Φ_i. Data for the aged Au-based ribbon in the present work are compared to those for other MGs $Zr_{55}Al_{10}Ni_5Cu_{30}$ [7], $Mg_{59.5}Cu_{22.9}Ag_{6.6}Gd_{11}$ [12], $Zr_{50}Cu_{40}Al_{10}$ [11], $Pd_{42.5}Cu_{30}Ni_{7.5}P_{20}$ [11].

annealed samples in the present work is ~200, significantly higher than the values reached in earlier work. As expected, rejuvenation reduces both E and H. The greater reductions achieved in the present work are roughly as expected from the trend in the published results on other MGs (Fig. 8a,b).

Rejuvenation of a MG can be achieved by cryogenic thermal cycling (CTC). Instrumented indentation has been used to compare the effects of CTC and of annealing [27]. In that work, on a (Cu,Zr)-based BMG, two types of property were distinguished. Properties relating to the initial yield event (pop-in), the load F_y, pressure P_y and pop-in size Δh, are sensitive to CTC, and are taken to be associated with local *soft-spots* in the MG. Properties such as hardness H and indentation modulus E_r are barely affected by CTC and are taken to be associated with the relatively hard and rigid matrix of the MG. All the properties are affected by annealing.

We first compare the effects of TR with the (opposite) effects of annealing. The shift in the cumulative distribution curves for P_y as a result of TR (Fig. 4b) is similar to the difference between the curves for annealed and as-cast samples of the (Cu,Zr)-based BMG (Fig. S7a in Ref. [27]). The reduction in median P_y from the value for the aged/annealed state is, respectively 19% and 9% in these two cases. The shapes of the cumulative distribution curves for Δh for aged and thermally rejuvenated samples are very similar (Fig. 4c), respectively to the curves for annealed and as-cast samples of the (Cu,Zr)-based BMG (Fig. 2a in Ref. [27]). In each case, the reduction from the Δh values for the aged/annealed samples is largely for above-median values. At the third quartile, the reduction in Δh from the value for the aged/annealed state is 53% in each case.

The cumulative distribution curves for H and for E_r are similar in the two studies. While retaining roughly the same shape, the curves shift, to lower values upon TR (present work) and to higher values upon annealing [27]. The reduction in median H in the present case is 13%. In the latter case, the median H is 8% lower for the as-cast than for the annealed MG [27]. The values of E_r show qualitatively similar behaviour in all cases. Thus, the effects of TR are similar, but opposite, to the effects of annealing.

We now compare our TR of a RT-aged MG with rejuvenation of the as-cast MG achieved using CTC (10 RT–77 K cycles [27]). The effects of CTC and TR in shifting the cumulative distribution curves for P_y and Δh to lower values are similar. The median P_y is reduced by 10% on CTC (cf. 19% by TR). The third quartile Δh is reduced by 59% on CTC (cf. 53% by TR). The effects of CTC and TR on H and E_r are, however, dramatically different. CTC has very little effect on these properties, compared to the clear reductions in the median values already noted for TR.

In contrast to the limited action of CTC, the present instrumented-indentation study shows that TR has global, not just local, effects on MG properties. Changing the matrix of the MG, not just soft-spots, should of course be expected as a result of heating into the supercooled-liquid state. Despite the decoupling and memory effect

noted in §4.2, the rejuvenation in the present work can indeed be regarded as an effective reversal of the annealing effect of the long ageing at RT.

5. Conclusions

By annealing a metallic glass (MG) briefly at a temperature T_a above its glass-transition temperature T_g, its fictive temperature T_f is increased. This thermal rejuvenation (TR) is attractive for improving mechanical properties. The extent of TR increases with the ratio (Φ_c/Φ_i), where Φ_c is the cooling rate after the anneal and Φ_i is the effective cooling rate at which the treated MG was formed. Earlier reports of TR had a maximum (Φ_c/Φ_i) of $\sim 10^2$. We have extended this to $\sim 10^7$ by using fast differential scanning calorimetry (FDSC) to achieve Φ_c values as high as 5000 K s^{-1}, and by studying a Au-based MG aged for up to 10 years at RT to achieve Φ_i values as low as 6×10^{-4} K s^{-1}. The extent of TR is quantified as an increase in T_f and as an increase in the enthalpy of the MG. Our maximum achieved increases in T_f (85 K) and in enthalpy (1.2 kJ mol^{-1}) greatly exceed any previously reported by TR. By extending the study to lower values of T_a/T_g than explored before, we can distinguish two regimes, in which the extent of TR is limited by T_a or by Φ_c, the latter regime being the focus of earlier studies.

The T_f values achieved by TR are lower than those expected from the temperature-dependent α-relaxation time reported for the Au-based MG, and lower than those measured directly in as-cast samples. This reflects a decoupling of vitrification from α relaxation, and is related to observed memory effects arising from the broad spectrum of relaxation times for structural changes in MGs. While changes in T_f are useful in detecting overall relaxation and rejuvenation, the state of a MG cannot be characterized only by T_f.

The effects of TR on elastic modulus E and hardness H have been explored in earlier reports; we extend these studies to $\Phi_c/\Phi_i \approx 200$ and find decreases in E of 8% and in H of 13%, a greater degree of rejuvenation than achieved before, but in line with the expected trend. Another method of rejuvenation, cryogenic thermal cycling, does reduce the pressure P_y and pop-in size Δh associated the initial yield event in instrumented indentation but hardly affects E or H. In contrast, the broader effects of TR suggest that it affects the matrix of the MG, not just soft-spots. TR effectively reverses the effects of prior annealing, including the effects of long-term ageing at room temperature.

Declaration of Competing Interest

The authors declare that they have no known competing financial interests or personal relationships that could have appeared to influence the work reported in this paper.

Acknowledgements

This work was supported by the European Commission, Marie Skłodowska-Curie Actions, grant FP7-PEOPLE-2013-ITN-607080, 'VitriMetTech' (for CMM), and by the European Research Council, grant ERC-2015-AdG-695487, 'ExtendGlass' (for ALG and CMM). KG acknowledges support from the HEIF-Cranfield project on BMGs. The authors thank O.S. Houghton for experimental assistance and for useful discussions.

Supplementary materials

Supplementary materials associated with this article can be found online at https://doi.org/10.1016/j.nocx.2021.100062.

References

[1] A.L. Mulder, S. van der Zwaag, A. van den Beukel, Embrittlement and disembrittlement in amorphous Metglas 2826 A, Scripta Metall. 17 (1983) 1399–1402.
[2] R. Gerling, F.R. Schimansky, R. Wagner, Ductilization of brittle amorphous alloys and reversible changes of the free volume by thermal treatments, Scripta Metall. 22 (1988) 1291–1295.
[3] F.P. Schimansky, R. Gerling, R. Wagner, Thermally induced restoration of the ductility of brittle amorphous alloys, Mater. Sci. Eng. A 133 (1991) 328–331.
[4] G. Kumar, D. Rector, R.D. Conner, J. Schroers, Embrittlement of Zr-based bulk metallic glasses, Acta Mater. 57 (2009) 3572–3583.
[5] J. Saida, R. Yamada, M. Wakeda, Recovery of less relaxed state in Zr-Al-Ni-Cu bulk metallic glass annealed above glass transition temperature, Appl. Phys. Lett. 103 (2013) 221910.
[6] M. Wakeda, J. Saida, J. Li, S. Ogata, Controlled rejuvenation of amorphous metals with thermal processing, Sci. Rep. 5 (2015) 10545.
[7] J. Saida, R. Yamada, M. Wakeda, S. Ogata, Thermal rejuvenation in metallic glasses, Sci. Technol. Adv. Mater. 18 (2017) 152–162.
[8] R. Yamada, N. Tanaka, W. Guo, J. Saida, Crystallization behavior of thermally rejuvenated $Zr_{50}Cu_{40}Al_{10}$ metallic glass, Mater. Trans. 58 (2017) 1463–1468.
[9] G.V. Afonin, N.P. Kobelev, V.A. Khonik, S.V. Nemilov, Rejuvenation of a metallic and oxide glass by cooling from the supercooled liquid state at laboratory rates, Phys. Stat. Sol. RRL 1800167 (2018).
[10] W. Guo, R. Yamada, J. Saida, S. Lü, S. Wu, Thermal rejuvenation of a heterogeneous metallic glass, J. Non-Cryst. Solids 498 (2018) 8–13.
[11] R. Yamada, N. Tanaka, W. Guo, J. Saida, Rejuvenation behavior and new classification of β-relaxation region in Pd-based metallic glass, J. Soc. Mater. Sci Japan 68 (2019) 191–198.
[12] W. Guo, J. Saida, M. Zhao, S. Lü, S. Wu, Thermal rejuvenation of an Mg-based metallic glass, Metall. Mater. Trans. A 50 (2019) 1125–1129.
[13] Y.H. Kim, K.R. Lim, D.W. Lee, Y.S. Choi, Y.S. Na, Quenching temperature and cooling rate effects on thermal rejuvenation of metallic glasses, Met. Mater. Int. (2020), https://doi.org/10.1007/s12540-020-00797-4.
[14] S. Küchemann, P.M. Derlet, C. Liu, D. Rosenthal, G. Sparks, W.S. Larson, R. Maaß, Energy storage in metallic glasses via flash annealing, Adv. Funct. Mater. 28 (2018) 1805385.
[15] W. Ryu, R. Yamada, J. Saida, Tailored hardening of ZrCuAl bulk metallic glass induced by 2D gradient rejuvenation, NPG Asia Materials 12 (2020) 52.
[16] M. Wakeda, J. Saida, Heterogeneous structural changes correlated to local atomic order in thermal rejuvenation process of Cu-Zr metallic glass, Sci. Technol. Adv. Mater. 20 (2019) 632–642.
[17] X. Monnier, D. Cangialosi, B. Ruta, R. Busch, I. Gallino, Vitrification decoupling from α-relaxation in a metallic glass, Sci. Adv. 6 (2020) eaay1454.
[18] C.M. Meylan, Thermomechanical Processing of Metallic Glasses, Ph.D. Thesis, University of Cambridge, 2019.
[19] Yu.P. Ivanov, C.M. Meylan, N.T. Panagiotopoulos, K. Georgarakis, A.L. Greer, In-situ TEM study of the crystallization sequence in a gold-based metallic glass, Acta Mater. 196 (2020) 52–60.
[20] K.L. Johnson, Contact Mechanics, Cambridge University Press, Cambridge, 1985.
[21] J. Schroers, B. Lohwongwatana, W.L. Johnson, A. Peker, Gold based bulk metallic glass, Appl. Phys. Lett. 87 (2005), 061912.
[22] J.S. Field, M.V. Swain, A simple predictive model for spherical indentation, J. Mater. Res. 8 (1993) 297–306.
[23] Q. Yang, S.X. Peng, Z. Wang, H.B. Yu, Shadow glass transition as a thermodynamic signature of β relaxation in hyper-quenched metallic glasses, Nat. Sci. Rev. 7 (2020) 1896–1905.
[24] C.M. Meylan, J. Orava, A.L. Greer, Rejuvenation through plastic deformation of a La-based metallic glass measured by fast scanning calorimetry, J. Non-Cryst. Solids: X 8 (2020) 100051.
[25] C.T. Moynihan, A.J. Easteal, M.A. DeBolt, J. Tucker, Dependence of the fictive temperature of glass on cooling rate, J. Am. Ceram. Soc. 59 (1976) 12–16.
[26] J.H. Perepezko, S.D. Imhoff, M.W. Chen, J.Q. Wang, S. Gonzalez, Nucleation of shear bands in amorphous alloys, Proc. Natl. Acad. Sci. U. S. A. 111 (2014) 3938–3942.
[27] C.M. Meylan, F. Papparotto, S. Nachum, J. Orava, M. Miglierini, V. Basykh, J. Ferenc, T. Kulik, A.L. Greer, Stimulation of shear-transformation zones in metallic glasses by cryogenic thermal cycling, J. Non-Cryst. Solids 548 (2020) 120299.
[28] C.E. Packard, O. Franke, E.R. Homer, C.A. Schuh, Nanoscale strength distribution in amorphous vs crystalline metals, J. Mater. Res. 25 (2010) 2251–2263.
[29] A.L. Greer, J.A. Leake, Structural relaxation and crossover effect in a metallic glass, J. Non-Cryst. Solids 33 (1979) 291–297.
[30] C. Scalliet, L. Berthier, Rejuvenation and memory effects in a structural glass, Phys. Rev. Lett. 122 (2019) 255502.
[31] L. Song, W. Xu, J. Huo, F. Li, L.-M. Wang, M.D. Ediger, J.-Q. Wang, Activation entropy as a key factor controlling the memory effect in glasses, Phys. Rev. Lett. 125 (2020) 135501.
[32] M. Philipp, C. Nies, M. Ostermeyer, W. Possart, J.K. Krüger, Thermal glass transition beyond kinetics of a non-crystallizable glass-former, Soft Matt. 14 (2018) 3601–3611.

[33] C.A. Angell, Formation of glasses from liquid and biopolymers, Science 267 (1995) 1924–1935.
[34] G.V. Afonin, O.A. Zamyatin, E.V. Zamyatina, V.A. Khonik, Thermal rejuvenation of tellurite glasses by cooling from the supercooled liquid state at low rates, Scripta Mater. 186 (2020) 39–42.
[35] Z.J. Evenson, On the Thermodynamic and Kinetic Properties of Bulk Glass Forming Metallic Systems, Dissertation, Univ. Saarland, 2012.

2021-06-02

Thermal rejuvenation of an aged Au-based metallic glass by fast scanning calorimetry

Meylan, C. M.

Elsevier

Meylan CM, Georgarakis K, Greer AL. (2021) Thermal rejuvenation of an aged Au-based metallic glass by fast scanning calorimetry. Journal of Non-Crystalline Solids: X, Volumes 11-12 (September-December 2021, Article number 100062

https://doi.org/10.1016/j.nocx.2021.100062